Accepted Manuscript
Version of record at: https://doi.org/10.1039/D1CP05765K

Factors influencing hydrogen peroxide versus water inclusion in molecular crystals†

Ren A. Wiscons,[a] Rahul Nikhar,[b]
Krzysztof Szalewicz*[b] and Adam J. Matzger*[a]

Abstract

Hydrate formation is often unavoidable during crystallization, leading to performance degradation of pharmaceuticals and energetics. In some cases, water molecules trapped within crystal lattices can be substituted for hydrogen peroxide, improving the solubility of drugs and detonation performance of explosives. The present work compares hydrates and hydrogen peroxide solvates in two ways:(1) analyzing structural motifs present in crystal structures accessed from the Cambridge Structural Database and (2) developing potential energy surfaces for water and hydrogen peroxide interacting with functional groups of interest at geometries relevant to the solid state. By elucidating fundamental differences in local interactions that can be formed with molecules of hydrogen peroxide and/or water, the analyses presented here provide a foundation for the design and selection of candidate molecules for the formation of hydrogen peroxide solvates.

1. Introduction

The formation of crystalline hydrates is a ubiquitous phenomenon in solid-state chemistry. Hydrates are crystalline materials in which molecules of water occupy defined positions within the crystal lattice, whether an isolated site or a channel.[1] Though the propensity to form hydrates can be exploited productively in salt-based desiccants, such as $MgSO_4$ and $CaCl_2$, the impact of hydrate formation on properties relevant to the performance of pharmaceuticals[1] and energetic materials[2,3] is almost always deleterious. Hydrates often show inferior aqueous solubility when compared to the corresponding anhydrate due to partial solvation in the hydrate form;[1,4] the formation of hydrates is accompanied by an increase in hydrogen bonding interactions that can stabilize the undesired hydrate form and reduce bioavailability of active pharmaceutical ingredients. However, hydrate formation during manufacturing, production, and storage often cannot be avoided. Despite the well precedented negative impact on bioavailability, ~20% of top drugs are crystalline hydrate forms.[1] Unintended hydrate formation also occurs in the area of explosives, where performance degradation is inevitable. In fact, we are aware of no hydrates of explosives that are fielded in any significant application. As an example, 5,5′-dinitro-2*H*,2*H*′-3,3′-bi-1,2,4-triazole (DNBT) can exist in an unprecedented six hydration states and the performance of each of these forms is reduced by the decrease in crystal density imparted by hydrate formation;[3] DNBT has yet to see use in commercial or military applications.

Hydrates make up more than 28% of all multicomponent organic crystal structures published in the Cambridge Structural Database (CSD), only 10% less than all other solvate forms combined.[5] The high occurrence of crystalline hydrates is due not only to the ubiquity of water during crystallization, but also the molecular structure of water itself, which offers both strong hydrogen bond donating and accepting sites in a compact molecule capable of occupying relatively small voids within a crystal. Recently, the detonation performance of the energetic 2,4,6,8,10,12-hexanitro-2,4,6,8,10,12-hexaazoisowurtzitane (CL-20) was improved through substitution of waters occupying structural cavities within α-CL-20 (CL-20 hydrate) for hydrogen peroxide, increasing the crystallographic density and improving the balance of fuel and oxidant.[2,6] Similarly, the antifungal miconazole forms a hydrogen peroxide solvate with improved aqueous solubility relative to both the hydrate and anhydrate forms in citrate-phosphate buffer.[7] However, the difficulty in applying hydrogen peroxide solvation as a general strategy to improve solid-state properties is that there is not yet a quantitative understanding of intermolecular interactions between hydrogen peroxide and functional groups to the extent that there is for water.

One route towards identifying systems likely to form hydrogen peroxide solvates is to substitute molecules of water in known hydrate crystal structures for molecules of hydrogen peroxide to form a structurally similar hydrogen peroxide

[a]Department of Chemistry and the Macromolecular Science and Engineering Program, University of Michigan, 930 North University of Ave, Ann Arbor, Michigan 48109-1055, USA. E-mail: matzger@umich.edu
[b]Department of Physics and Astronomy, University of Delaware, Newark, Delaware, 19716, USA. E-mail: szalewic.@udel.edu
† Electronic supplementary information (ESI) available. See DOI: https://doi.org/ 10.1039/d1cp05765k

solvate (*i.e.*, isomorphous/isostructural replacement).[8] Isomorphous substitution of water molecules for molecules of hydrogen peroxide has been investigated in depth for small molecules published in the CSD, leading to a list of conditions necessary to produce hydrogen peroxide solvates isomorphous to the parent hydrate crystal structure.[8] However, while there are several examples in which molecules of water have been substituted to produce structurally-related hydrogen peroxide solvates, not all peroxide solvates are crystallographically isomorphous to their parent hydrates. Hydrogen peroxide solvates that are not isomorphous to the hydrate form of the parent compounds can better exclude water as the conversion to the corresponding hydrate would require reorganization of the crystal lattice. As a result, hydrogen peroxide solvates that are not isomorphous to the hydrate form of the parent compound are predicted to provide solubility advantages for pharmaceuticals, lowered hygroscopicity of salt solvates, and improved detonation performance for energetics. Additionally, compounds that produce hydrogen peroxide solvates that lack isomorphous hydrates, such as urea and melamine, may be crystallized selectively from dilute hydrogen peroxide solutions with minimal incorporation of water.[8] These advantages further motivate the development of hydrogen peroxide solvate design criteria that do not rely on crystallographic isomorphism.

Here we present strategies towards designing hydrogen peroxide solvates grounded in interaction energy differences between water or hydrogen peroxide and functional groups of interest. This is achieved by determining interaction enthalpies between water or hydrogen peroxide and various functional groups at points on potential energy surfaces (PESs) representing crystallographically-relevant interaction geometries. From these interaction enthalpy differences, we have developed actionable strategies to filter and target coformers with a high probability of forming hydrogen peroxide solvates selectively. This study is organized in the following sections: Section 2.1 compares interaction geometries between hydrogen peroxide or water and various functional groups extracted from representative crystal structures obtained from the CSD. Section 2.2 compares interaction energies between water or hydrogen peroxide with several model molecules (methanol, formamide, pyridine-*N*-oxide, nitromethane, methylamine, and imidazole) at dimer configurations selected to represent the experimental crystallographic geometries. The results of these studies include actionable recommendations of functional groups likely to favor hydrogen peroxide solvate formation.

2. Results and discussion

2.1 Crystallographic interaction geometries

Interaction selectivities in crystals arise mainly from differences in interaction energies. For example, a difference in interaction energy of 1.36 kcal mol^{-1} leads to a 10 : 1 selectivity advantage in favor of the more thermodynamically stable interaction. For this reason, calculating the interaction energies of water or hydrogen peroxide with specific functional groups can provide a prediction for whether a compound is more or less selective for interaction with hydrogen peroxide over water. However, interaction energies are sensitive to the interaction geometry and relatively small changes in geometry can lead to energy differences on the order of a few kcal mol^{-1}, necessitating careful selection of interaction geometries for comparison. The interaction geometries present in crystal structures represent a compromise between several thermodynamic contributions, such as competing local interactions, steric constraints, and long-range packing forces. Due to the additional interaction sites offered by a molecule of hydrogen peroxide compared to a molecule of water, the interactions involving hydrogen peroxide in the solid state are subject to competition with a greater number of local interactions, leading to individual interaction geometries that are expected to be further from gas-phase geometries than those observed for water in the solid state. For these reasons, computational determination of interaction enthalpies for water or hydrogen peroxide with model molecules at gas-phase global minimum energy geometries yields values that may not be appropriate estimates of interaction selectivities in the solid state. A more relevant approach is to compute interaction energies between water or hydrogen peroxide and model compounds at dimer configurations that represent average crystallographic geometries. These configurations are not, in general, minima on the PESs.

In order to develop design principles for the discovery of hydrogen peroxide solvates based on interaction selectivities, hydrogen bonding enthalpies at crystallographically relevant geometries must be determined. Such geometries were found by measuring average intermolecular interaction distances and approach angles between molecules of water or hydrogen peroxide and select functional group classes from crystal structures deposited in the CSD (November 2018, v.5.40) and filtered using a combination of IsoStar (2018, v2.3) and substructure similarity searches using ConQuest (v2.0.0) offered through the Cambridge Crystallographic Data Centre. The statistics presented in this study are based on 179 interaction geometries in 136 crystal structures (see ESI†). Each crystal structure was inspected for structure quality and disorder prior to measurement. Given the uncertainty associated with locating hydrogen atoms by single-crystal X-ray diffraction (SCXRD), all hydrogen bonding distances were measured as donating heteroatom···accepting heteroatom, d(O···O/N). Specific geometric parameters were measured to describe the interaction approach angle and direction with the goal of determining an average interaction geometry between water or hydrogen peroxide and target functional groups in the solid state. Discussion of measured functional groups is divided into two sections: oxygen-containing (Section 2.1(a)) and nitrogen-containing (Section 2.1(b)) hydrogen bond accepting groups. Following these two sections is a brief discussion comparing the relative hydrogen bond accepting strengths of water and hydrogen peroxide (Section 2.1(c)).

2.1(a). Oxygen-containing hydrogen bond accepting groups. The most diverse class of functional groups measured for this study is comprised of oxygen atom-containing hydrogen bond accepting groups. This class includes aliphatic and aromatic alcohol (as a hydrogen bond acceptor), carbonyl, *N*-oxide, and

Accepted Manuscript
Version of record at: https://doi.org/10.1039/D1CP05765K

nitro groups. The results of this study are listed in Tables S2–S8 and summarized in Table S13 (ESI†). In addition, Table S1 (ESI†) shows results for alcohols interacting as donors with water (these results will not be discussed in what follows). On average, hydrogen peroxide shows shorter d(O···O) contacts than does water, with the exception of the nitro group, for which the respective distances are 2.889(8) and 3.037 Å. Because there is only one ordered interaction example between nitro groups and hydrogen peroxide in the CSD, no average is involved in this case (a quantitative geometric description of this structure is given in Table S13 of the ESI†). As a hydrogen bond donor, hydrogen peroxide shows an average interaction distance (standard errors of the mean are given in parentheses) to alcohol, carbonyl, and *N*-oxide groups of 2.75(8), 2.72(5), and 2.70(1) Å, while the corresponding distances for water are 2.775(2), 2.808(9), and 2.752(2) Å. The shorter distances for hydrogen bonds donated by hydrogen peroxide relative to water are consistent with the increase in acidity of hydrogen peroxide (pK_a = 11.6)[9] relative to water (pK_a = 14.0)[10] and is predictive of larger interaction enthalpies.

In addition to interaction distances, the approach angles and dihedrals defining the interaction geometries between water or hydrogen peroxide and the various functional groups were also measured. The geometric measurements are consolidated into three angular/dihedral parameters (Fig. 1) in 3D space to illustrate the dispersity of approach geometries tabulated from crystal structures for each functional group with water and hydrogen peroxide. The degree of clustering of data points on the 3D plots is indicative of the specificity along the measured angular and/or torsional parameters used to define the approach of water or hydrogen peroxide to each functional group. For example, the 3D interaction plot summarizing the approach geometries of water and hydrogen peroxide to alcohol functional groups shows that the ∠(C–O···O) approach angle exhibits relatively tight clustering, whereas the ∠(C–C–O···O) dihedrals can vary substantially across the crystal structures (Fig. 1A). This observation is interpreted as the water or hydrogen peroxide approach angle being restricted to an angle of 120(10)° with respect to the alcohol oxygen atom, but the approach direction is otherwise unspecific. Comparatively, geometries measured from crystal structures featuring interaction of water or hydrogen peroxide with *N*-oxide groups (Fig. 1B) show unspecific approach angles and approach dihedrals as shown by the scatter of the data along the ∠(N–O···O) angle and the ∠(C–N–O···O)$_{short}$ dihedral, indicating that the approach geometry is less selective than that measured for interaction with alcohol functional groups.

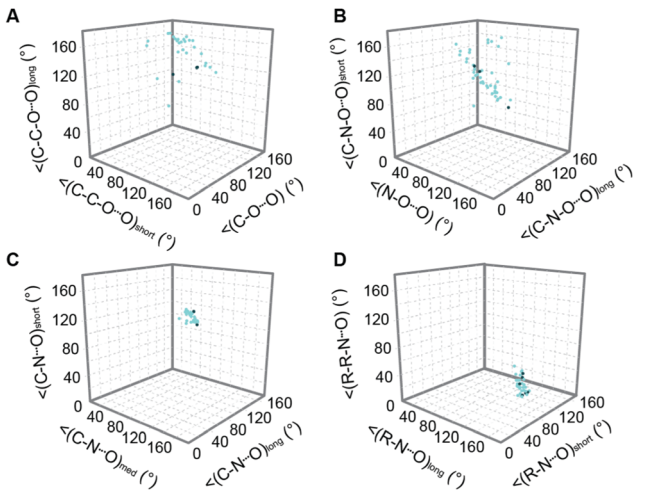

Fig. 1 3D interaction plots describing the distribution of approach angles of water (light blue) and hydrogen peroxide (dark blue) towards (A) alcohol, (B) *N*-oxide, (C) sp^3 nitrogen, and (D) sp^2 nitrogen functional groups measured from crystal structures. The absolute values of all geometric parameters are shown. Definitions for geometric parameters are given in the ESI.†

2.1(b). Nitrogen-containing hydrogen bond accepting groups. The interaction geometries between water or hydrogen peroxide and sp^3 amine groups or sp^2 hybridized nitrogen atoms (primarily nitrogen-containing heterocycles) were investigated by measuring the interaction distances, angles, and dihedrals present in X-ray crystal structures accessed from the CSD. The results are listed in Tables S9–S12 and summarized in Table S14 (ESI†). On average, hydrogen bonds donated from water or hydrogen peroxide to nitrogen-centered acceptors are approximately 0.1 Å longer than those donated to oxygen-centered acceptors, which is consistent with the increase in van der Waals radius from oxygen to nitrogen. Similarly to the oxygen-containing hydrogen bond accepting groups, hydrogen peroxide shows shorter average d(O···N) than water, with hydrogen bonding distances to sp^3 hybridized nitrogen atoms of 2.78(7) Å and to sp^2 hybridized nitrogen atoms of 2.76(3) Å, while the corresponding distances for interaction with water are 2.908(6) Å and 2.884(8) Å. These data again suggest stronger interaction in the hydrogen peroxide-containing heterodimers. The 3D interaction plots generated from the interaction angle parameters for the amine and aromatic nitrogen-containing functional groups (Fig. 1C and D) demonstrate tight clustering of the data points, suggesting that the interaction approach angles and directions for these functional groups with water or hydrogen peroxide are more predictable than those measured for oxygen-centered functional groups, likely due to the well-defined positions and/or localization of electron density present in sp^3 and sp^2 hybridized nitrogen functional groups when compared to the oxygen-containing hydrogen bond accepting groups measured in the previous section.

2.1(c). Water *versus* hydrogen peroxide as hydrogen bond acceptors. It is well-established that, at the global energy minima for interaction between identical hydrogen bond acceptors, hydrogen peroxide is a stronger hydrogen bond donor than is water. The data presented here shows that this trend persists in the crystallographically relevant geometries. That said, the relative strength of water and hydrogen peroxide serving as hydrogen bond acceptors is less well explored. Two crystal structures (GADOXP10 and KELXAD) were selected to investigate the relative interaction strength between hydrogen peroxide and water as hydrogen bond acceptors. These crystal structures feature hydrogen bonding interactions between a hydrogen peroxide homodimer and a hydrogen peroxide and water heterodimer in which water is the hydrogen bond acceptor.

Accepted Manuscript
Version of record at: https://doi.org/10.1039/D1CP05765K

The crystal structure featuring hydrogen peroxide homodimers shows hydrogen bonding distances as short as 2.675 Å (and as long as 2.784 Å), while that of the hydrogen peroxide and water heterodimer is 2.667 Å. Because hydrogen peroxide is the hydrogen bond donor in both cases, these data suggest that water is a stronger hydrogen bond acceptor than is hydrogen peroxide. This prediction is further supported by the interaction energy difference between the hydrogen peroxide homodimer and the hydrogen peroxide and water heterodimer at the experimental interaction geometries, which is calculated at 1.3 kcal mol^{-1} in favor of the hydrogen peroxide and water heterodimer.

2.2 Determination of PESs and interaction energies

The autoPES software package[11] was used to generate PESs for molecules of water or hydrogen peroxide interacting with various small model molecules (methanol, formamide, pyridine-*N*-oxide, nitromethane, methylamine, and imidazole) representing the functional groups under consideration (alcohol, amide, *N*-oxide, nitro, sp^3 amine, and sp^2 nitrogen). Full details of the PES generation are available in the ESI.† The PESs were used to determine the equilibrium configurations of the dimers and to find the values of the coordinates in experimental geometries that were not measured. All the interaction energies and their components at these configurations were computed *ab initio*. Section VI of the ESI† discusses the accuracies of the fits. The *ab initio* optimized molecular geometries for water,[12] hydrogen peroxide,[13] and formamide[14] used for this study were obtained from literature. Monomer geometries for methanol, pyridine-*N*-oxide, nitromethane, methylamine, and imidazole were optimized in the present work at the second-order of many-body perturbation theory based on the Møller–Plesset partition of the Hamiltonian (MP2) and a triple-zeta quality basis (aug-cc-pVTZ)[15] using the Gaussian09[16] codes. Interaction energies between heterodimers of water or hydrogen peroxide and the small model molecules were computed using symmetry adapted perturbation theory[17] based on density functional theory descriptions of monomers SAPT(DFT)[18–28] using the SAPT codes[29] interfaced with the ORCA electronic structure package.[30] The total interaction energy is defined as the sum of the following contributions:

$$E_{\mathrm{int}} = E^{(1)}_{\mathrm{elst}} + E^{(1)}_{\mathrm{exch}} + E^{(2)}_{\mathrm{ind}} + E^{(2)}_{\mathrm{exch\text{-}ind}} + E^{(2)}_{\mathrm{disp}} + E^{(2)}_{\mathrm{exch\text{-}disp}} + \delta E^{\mathrm{HF}}_{\mathrm{int,resp}}$$

where the superscripts denote the order of perturbation with respect to the intermonomer interaction operator. The electrostatic interaction contribution, denoted by $E^{(1)}_{\mathrm{elst}}$, is the Coulomb interaction between unperturbed charge distributions of the interacting monomers. The first-order exchange energy (exchange-repulsion energy), denoted by $E^{(1)}_{\mathrm{exch}}$, results from the antisymmetrization of the product of unperturbed monomer wave functions and may be viewed as ''Pauli repulsion'' of electron charge distribution. The induction energy, denoted by $E^{(2)}_{\mathrm{ind}}$, results from deformations of the monomer wave functions by the electrostatic field of the interacting partner. The dispersion energy, denoted by $E^{(2)}_{\mathrm{disp}}$, results from long-range correlations between electrons of monomer A and those of monomer B. The exchange-induction (exchange-dispersion) energy, denoted by $E^{(2)}_{\mathrm{exch\text{-}ind}}$ ($E^{(2)}_{\mathrm{exch\text{-}disp}}$), results from the antisymmetrization of the induction (dispersion) wave functions. In this study, the $\delta E^{\mathrm{HF}}_{\mathrm{int,resp}}$ [31,32] term was included primarily to account for induction and exchange-induction effects beyond second order (see ESI† for additional details). To simplify discussion of physical components, we have grouped some corrections denoting $E_{\mathrm{indx}} = E^{(2)}_{\mathrm{ind}} + E^{(2)}_{\mathrm{exch\text{-}ind}} + \delta E^{\mathrm{HF}}_{\mathrm{int,resp}}$ and $E^{(2)}_{\mathrm{dispx}} + E^{(2)}_{\mathrm{isp}} + E^{(2)}_{\mathrm{exch\text{-}disp}}$.

Fig. 2 shows dimers in the global minimum configurations on each surface. Since such configurations are not necessarily close to the configurations present in crystals, we have also computed SAPT interaction energies with dimer parameters fixed at the average experimental values from Tables S13 and S14 (ESI†). These geometries are shown in Fig. 3. As these structures are not minima on the PESs, we refer to them as ''near-experimental geometries''. A detailed description of constructing the near-experimental dimer configurations is given in ESI.†

The PES geometries selected to represent the experimental geometries, Fig. 3, are generally not expected to be the same as the geometries at the global minimum energies, Fig. 2, due to competing local and long-range interactions. However, comparison of Fig. 2 and 3 shows that in some cases the near-experimental geometries are reasonably close to the global minima geometries. In particular, all hydrogen bonds are in approximately the same locations except for heterodimers formed with formamide and nitromethane, where the global minimum structures are doubly hydrogen bonded, while the near-experimental ones are not. The interaction geometries of

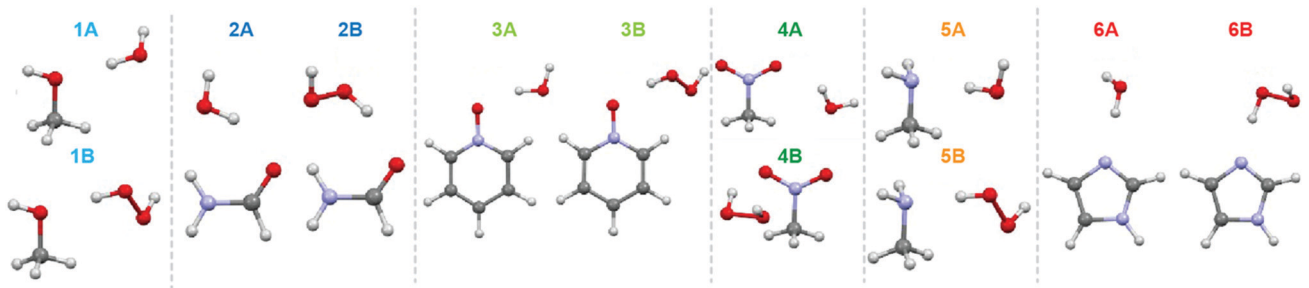

Fig. 2 PES global minimum geometries for heterodimers formed between water (A) or hydrogen peroxide (B) and the small molecule models: methanol (1), formamide (2), pyridine oxide (3), nitromethane (4), methylamine (5), and imidazole (6).

Accepted Manuscript
Version of record at: https://doi.org/10.1039/D1CP05765K

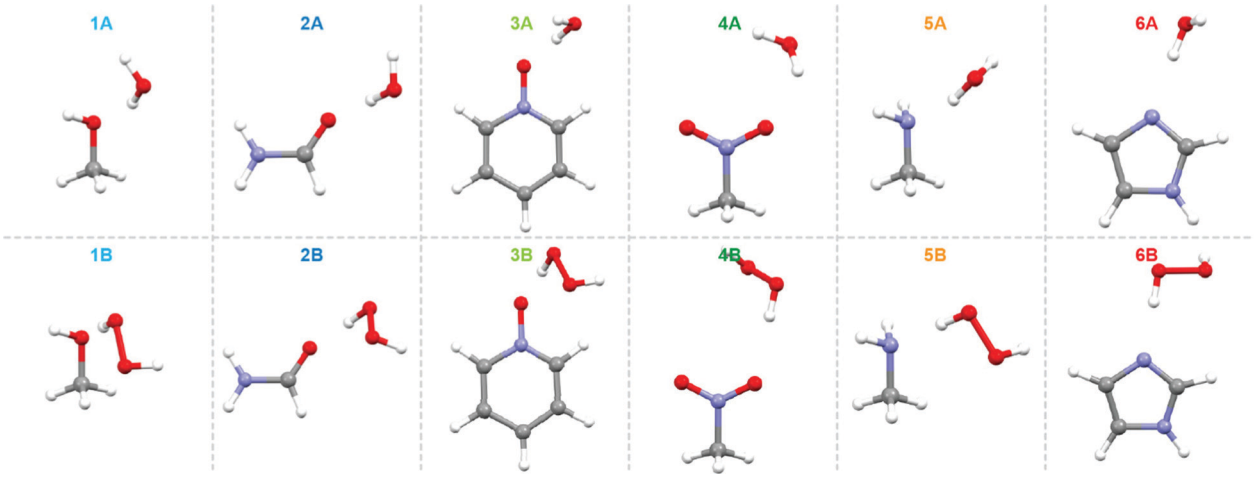

Fig. 3 Interaction geometries of heterodimers between water or hydrogen peroxide and the small molecule models at near-experimental dimer configurations based on average interaction geometries extracted from crystal structures (see text). The color of the structure label indicates the functional group class represented by the model molecule: light blue text indicates alcohol functional groups, dark blue is carbonyl, light green is *N*-oxide, dark green is nitro, orange is sp^3 nitrogen, and red is sp^2 nitrogen.

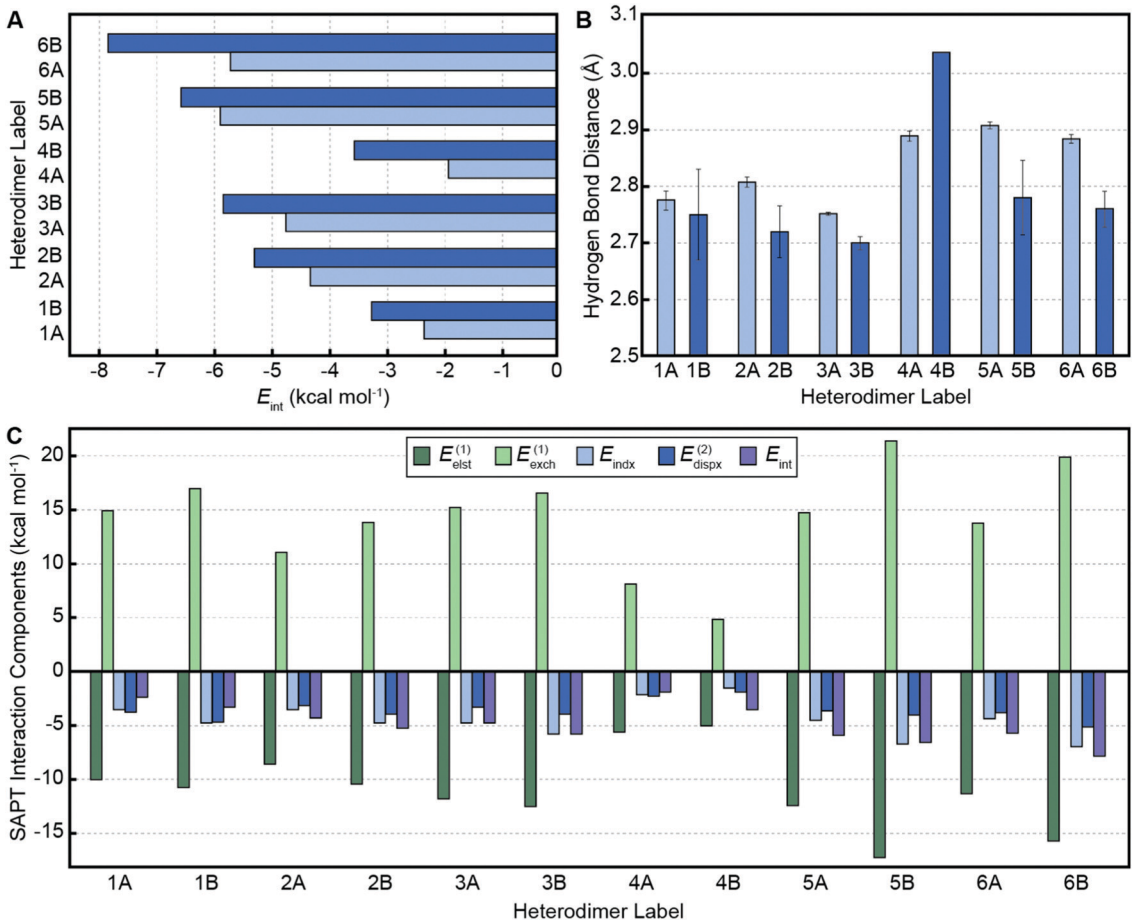

Fig. 4 (A) SAPT interaction energy comparison for model molecules (defined in Fig. 2 and 3) interacting with water (light blue) or hydrogen peroxide (dark blue) at near-experimental geometries; (B) average interaction distances between water or hydrogen peroxide and various functional groups measured from crystal structures with error bars representing the standard error of the mean; (C) analysis of the components of SAPT energies for the near-experimental geometries used for model molecules interacting with water or hydrogen peroxide.

four pairs of structures are nearly identical between the global minimum structures and the near-experimental geometries: water with methanol and hydrogen peroxide with pyridine-*N*-oxide, methylamine, and imidazole.

In general, the small model molecules were found to form more favorable hydrogen bonding interactions with hydrogen peroxide than with water at near-experimental geometries, as shown in Fig. 4A. Specifically, the dimers containing hydrogen peroxide have more favorable SAPT interaction energies by 0.9, 1.0, 1.1, 1.6, 0.7, and 2.1 kcal mol^{-1} for methanol, formamide, pyridine-*N*-oxide, nitromethane, methylamine, and imidazole, respectively, than for the analogous heterodimers formed with water. These energy differences predict that molecules containing sp^2 nitrogen functional groups will show the strongest selectivities for hydrogen peroxide over water interaction. The SAPT energy differences at PES minimum geometries show a similar trend (see ESI†), in particular the heterodimer containing the sp^2 nitrogen shows again the largest energy difference in favor of interaction with hydrogen peroxide, 3.3 kcal mol^{-1}. The trend in relative interaction strength between hydrogen peroxide and water-containing heterodimers is consistent with the shorter average interaction distances between hydrogen peroxide and the various functional groups compared to the water counterparts measured from crystal structures (Fig. 4B). In particular, the average d(O$\cdots$N) for sp^2 nitrogen has the second largest difference in hydrogen bonding distance (0.124 Å shorter with hydrogen peroxide) and was calculated to have the largest difference in total SAPT interaction energy (2.1 kcal mol^{-1}). On the other hand, sp^3 functional group has the largest difference in hydrogen bonding distance (0.128 Å shorter for hydrogen peroxide), but has the smallest SAPT energy difference (0.7 kcal mol^{-1}). However, at PES minima, which are very similar to near-experimental minima for sp^3, the energy difference is the second largest. The only significant exceptions are dimers involving nitro groups where the hydrogen bond is shorter for the dimer with water (but the interaction energy is still larger in magnitude for the interactions with hydrogen peroxide). At PES minima, however, these dimers are not outliers. The reason is likely that near-experimental geometry of a nitro group interaction with hydrogen peroxide is based only on one crystal structure.

The components of the SAPT interaction energies are shown in Fig. 4C. As the intermolecular distance between monomers shortens, both the attractive and repulsive components increase in magnitude. This relationship explains the correlation between Fig. 4B and C (*i.e.*, shorter bonds roughly correlate with larger magnitudes of components). For all of the heterodimers containing the model molecules, the dominant attractive term is the electrostatic energy, as the contribution of the dispersion and induction energy terms are 2–3 times smaller in magnitude. However, the electrostatic contribution is almost completely cancelled by the exchange energy in each case. Consequently, the hydrogen bond is a combined effect of all the interaction energy components, and not just the electrostatic interactions of the permanent charge distributions. It is found that the relative contributions of the electrostatic, induction, and dispersion components are not significantly different for hydrogen peroxide *versus* water containing dimers, but all these components are larger in magnitude in the former case, leading to the observed more attractive interaction energy in favor of hydrogen peroxide. Additional discussion of interaction energy components is provided in the ESI.†

3. Conclusions

Selective interaction with hydrogen peroxide over water at crystallographically relevant interaction geometries has been predicted for a variety of functional group classes. Based on PESs generated for these systems and SAPT interaction energies, dimers containing hydrogen peroxide were found to have larger magnitudes of interaction energy and shorter hydrogen bond lengths than the corresponding dimers with water, both at the global PES minima and at the near-experimental geometries. Interactions involving the nitro groups are the only exceptions, which is likely due to the limited number of experimental structures featuring hydrogen bonds between nitro groups and hydrogen peroxide; in fact, at PES minima the interactions involving the nitro groups are consistent with other functional groups considered. All the geometries exhibit hydrogen bonding interactions and all of the interaction energy components given by SAPT play a significant role in determining the strength of interactions, not simply the electrostatic contribution to the interaction energies.

Several design strategies are proposed to improve the likelihood of forming hydrogen peroxide solvates. Consistent with previous experimental and computational work, hydrogen peroxide is a stronger hydrogen bond donor than water in both the PES minima and in the crystallographically-relevant geometries. We have also presented a set of crystal structures that suggests water is a stronger hydrogen bond acceptor than is hydrogen peroxide. For this reason, candidate molecules for hydrogen peroxide solvate formation should not simply be selected based on hydrogen bond formation, but whether the hydrogen bonds possibly donated by hydrogen peroxide are predicted to be stronger than those that can be accepted by water. Overall, the sp^2 nitrogen functional group showed the greatest selectivity for hydrogen peroxide over water at crystallographically relevant geometries, exhibiting greater than a 10 : 1 selectivity based on the total interaction energy. This group is the strongest candidate for hydrogen peroxide solvate formation because (1) it shows the largest interaction energy differences, on average, in favor of hydrogen peroxide in the crystallographic geometries; (2) there are structural analogues of these functional groups in which there is no competition with hydrogen bond donation by the candidate molecule; and (3) there are strongly conserved interaction approach geometries for this functional group, as shown by the 3D interaction plots, suggesting that the computed selectivity advantages for hydrogen peroxide should be general across most crystal structures containing sp^2 nitrogen functional group.

Author contributions

R. A. W. performed structural motifs analysis, R. N. performed SAPT(DFT) calculations and developed PESs for model

molecules with water/hydrogen peroxide heterodimers; K. S. and A. J. M. supervised the research. All authors discussed the progress of the research and reviewed the manuscript.

Conflicts of interest

There are no conflicts to declare.

Acknowledgements

This work was supported by the Army Research Office under grants W911NF-13-1-0387, W911NF-19-0114, W911NF-19-0117, and DURIP W911NF-16-0167 and National Science Foundation under grant CHE-1900551.

References

1 J. T. Damron, K. M. Kersten, M. K. Pandey, Y. Nishiyama, A. J. Matzger and A. Ramamoorthy, *ChemistrySelect*, 2017, **2**, 6797–6800.
2 J. C. Bennion, N. Chowdhury, J. W. Kampf and A. J. Matzger, *Angew. Chem., Int. Ed.*, 2016, **55**, 13118–13121.
3 R. A. Wiscons, M. K. Bellas, J. C. Bennion and A. J. Matzger, *Cryst. Growth Des.*, 2018, **18**, 7701–7707.
4 R. K. Khankari and D. J. W. Grant, *Thermochim. Acta*, 1995, **248**, 61–79.
5 K. M. Kersten, R. Kaur and A. J. Matzger, *IUCrJ*, 2018, **5**, 124–129.
6 V. S. Vuppuluri, J. C. Bennion, R. A. Wiscons, I. E. Gunduz, A. J. Matzger and S. F. Son, *Propellants, Explos., Pyrotech.*, 2019, **44**, 313–318.
7 K. M. Kersten, M. E. Breen, A. K. Mapp and A. J. Matzger, *Chem. Commun.*, 2018, **54**, 9286–9289.
8 I. Y. Chernyshov, M. V. Vener, P. V. Prikhodchenko, A. G. Medvedev, O. Lev and A. V. Churakov, *Cryst. Growth Des.*, 2017, **17**, 214–220.
9 D. M. Davies and M. E. Deary, *J. Chem. Soc., Perkin Trans. 2*, 1991, 1549–1552.
10 E. C. Meister, M. Willeke, W. Angst, A. Togni and W. P. Helv, *J. Chem. Theory Comput.*, 2012, **8**, 1963–1969.
11 M. P. Metz, K. Piszczatowski and K. Szalewicz, *J. Chem. Theory Comput.*, 2016, **12**, 5895–5919.
12 E. M. Mas and K. Szalewicz, *J. Chem. Phys.*, 1996, **104**, 7606–7614.
13 P. Małyszek and J. Koput, *J. Comput. Chem.*, 2013, **34**, 337–345.
14 J. S. Kwiatkowski and J. Leszczyński, *J. Mol. Struct.*, 1993, **297**, 277–284.
15 R. A. Kendall, T. H. Dunning, Jr. and R. J. Harrison, *J. Chem. Phys.*, 1992, **96**, 6796–6806.
16 M. J. Frisch, G. W. Trucks, H. B. Schlegel, G. E. Scuseria, M. A. Robb, J. R. Cheeseman, G. Scalmani, V. Barone, B. Mennucci, G. A. Petersson, H. Nakatsuji, M. Caricato, X. Li, H. P. Hratchian, A. F. Izmaylov, J. Bloino, G. Zheng, J. L. Sonnenberg, M. Hada, M. Ehara, K. Toyota, R. Fukuda, J. Hasegawa, M. Ishida, T. Nakajima, Y. Honda, O. Kitao, H. Nakai, T. Vreven, J. A. Montgomery, Jr., J. E. Peralta, F. Ogliaro, M. Bearpark, J. J. Heyd, E. Brothers, K. N. Kudin, V. N. Staroverov, R. Kobayashi, J. Normand, K. Raghavachari, A. Rendell, J. C. Burant, S. S. Iyengar, J. Tomasi, M. Cossi, N. Rega, J. M. Millam, M. Klene, J. E. Knox, J. B. Cross, V. Bakken, C. Adamo, J. Jaramillo, R. Gomperts, R. E. Stratmann, O. Yazyev, A. J. Austin, R. Cammi, C. Pomelli, J. W. Ochterski, R. L. Martin, K. Morokuma, V. G. Zakrzewski, G. A. Voth, P. Salvador, J. J. Dannenberg, S. Dapprich, A. D. Daniels, O. Farkas, J. B. Foresman, J. V. Ortiz, J. Cioslowski and D. J. Fox, *Gaussian 09, Revision A.02*, 2009.
17 B. Jeziorski, R. Moszyński and K. Szalewicz, *Chem. Rev.*, 1994, **94**, 1887–1930.
18 H. L. Williams and C. F. Chabalowski, *J. Phys. Chem. A*, 2001, **105**, 646–659.
19 A. J. Misquitta and K. Szalewicz, *Chem. Phys. Lett.*, 2002, **357**, 301–306.
20 A. Hesselmann and G. Jansen, *Chem. Phys. Lett.*, 2002, **357**, 464–470.
21 A. Hesselmann and G. Jansen, *Chem. Phys. Lett.*, 2002, **362**, 319–325.
22 A. J. Misquitta, B. Jeziorski and K. Szalewicz, *Phys. Rev. Lett.*, 2003, **91**, 033291.
23 A. Hesselmann and G. Jansen, *Chem. Phys. Lett.*, 2003, **367**, 778–784.
24 A. J. Misquitta and K. Szalewicz, *J. Chem. Phys.*, 2005, **122**, 214109.
25 A. J. Misquitta, R. Podeszwa, B. Jeziorski and K. Szalewicz, *J. Chem. Phys.*, 2005, **123**, 214103.
26 A. Hesselmann, G. Jansen and M. Schütz, *J. Chem. Phys.*, 2005, **122**, 014103.
27 R. Bukowski, R. Podeszwa and K. Szalewicz, *Chem. Phys. Lett.*, 2005, **414**, 111–116.
28 R. Podeszwa, R. Bukowski and K. Szalewicz, *J. Chem. Theory Comput.*, 2006, **2**, 400–412.
29 R. Bukowski, W. Cencek, P. Jankowski, M. Jeziorska, B. Jeziorski, S. A. Kucharski, V. F. Lotrich, M. P. Metz, A. J. Misquitta, R. Moszyński, K. Patkowski, R. Podeszwa, F. Rob, S. Rybak, K. Szalewicz, H. L. Williams, R. J. Wheatley, P. E. S. Wormer and P. S. Żuchowski, *SAPT2016: An ab Initio Program for Many-Body Symmetry-Adapted Perturbation Theory Calculations of Intermolecular Interaction Energies*, University of Delaware and University of Warsaw, 2016, **https://www.physics.udel.edu/∼szalewic/SAPT**.
30 F. Neese, *Wiley Interdiscip. Rev.: Comput. Mol. Sci.*, 2012, **2**, 73–78.
31 M. Jeziorska, B. Jeziorski and J. Cizek, *Int. J. Quantum Chem.*, 1987, **32**, 149–164.
32 K. Patkowski, K. Szalewicz and B. Jeziorski, *J. Chem. Phys.*, 2006, **125**, 154107.